Journal of
Synchrotron Radiation

ISSN 0909-0495

Received 8 March 2007
Accepted 2 April 2007

Windowless transition between atmospheric pressure and high vacuum *via* differential pumping for synchrotron radiation applications

T. Gog,* D. M. Casa, I. Kuzmenko, R. J. Krakora and T. B. Bolin

CMC-XOR, Advanced Photon Source, Argonne National Laboratory, 9700 South Cass Avenue, Argonne, IL, USA. E-mail: gog@anl.gov

A differential pump assembly is introduced which can provide a windowless transition between the full atmospheric pressure of an in-air sample environment and the high-vacuum region of a synchrotron radiation beamline, while providing a clear aperture of approximately 1 mm to pass through the X-ray beam from a modern third-generation synchrotron radiation source. This novel pump assembly is meant to be used as a substitute for an exit vacuum window on synchrotron beamlines, where the existence of such a window would negatively impact the coherent nature of the X-ray beam or would introduce parasitic scattering, distorting weak scattering signals from samples under study. It is found that the length of beam pipe necessary to reduce atmospheric pressure to below 10 mbar is only about 130 mm, making the expected photon transmission for hard X-rays through this pipe competitive with that of a regular Be beamline window. This result is due to turbulent flow dominating the first pumping stage, providing a mechanism of strong gas conductance limitation, which is further enhanced by introducing artificial surface roughness in the pipe. Successive reduction of pressure through the transitional flow regime into the high-vacuum region is accomplished over a length of several meters, using beam pipes of increasing diameter. While the pump assembly has not been tested with X-rays, possible applications are discussed in the context of coherent and small-angle scattering.

Keywords: differential pump; X-ray window; coherent scattering; small-angle scattering.

1. Introduction

Advances in recent years in the field of third-generation synchrotron radiation sources have provided the researcher with ever brighter, smaller and dramatically more coherent X-ray beams. This has lead to the advent of new X-ray analytical techniques such as speckle, coherent diffraction, X-ray photon correlation spectroscopy, and other coherent techniques (Sutton, 2002) that were technically not feasible just a decade ago. While X-ray sources have undergone a vast improvement, a remaining challenge is to preserve the coherent characteristics of the X-ray beam as it traverses the various optical elements of the beamline on its way to the experimental station. One class of known offenders are vacuum windows, which usually provide the interface between the vacuum environment of the beamline or accelerator and the outside world. These windows are often not optically flat on the scale of an X-ray wavelength and thus can distort the wavefront of an X-ray beam passing through, increase its divergence, and thereby substantially degrade its coherent quality (Suzuki *et al.*, 1998; Snigirev *et al.*, 1996).

Another area which can benefit from the elimination of an exit window is small-angle X-ray scattering. Here, parasitic scattering from material windows often obscures signals from weakly scattering samples at low angles and thereby determines the smallest accessible scattering vector (Bösecke & Diat, 1997; Henderson, 1995; Jaski & Cookson, 2007).

Given advances in vacuum technology, combined with the small sizes of modern synchrotron beams, it appears feasible to eliminate vacuum windows for these special applications altogether and negotiate the gradient between the atmospheric pressure of an in-air sample environment and the high-vacuum region of the beamline or accelerator solely through differential pumping. This concept as such is not new. Indeed, a successful attempt has been made to pass micrometer-sized X-ray beams through differentially pumped glass capillaries (Nebiki *et al.*, 2006), and various facilities, for example soft X-ray photochemistry beamlines around the world, employ differentially pumped reaction chambers with allowable pressures of up to 1 mbar (Ohashi *et al.*, 2001). A windowless transition has also been achieved by means of a 'plasma window' (Hershcovitch, 1998; Hershcovitch *et al.*, 2003;

Pinkoski *et al.*, 2001), where a short plasma arc provides the separation between atmospheric pressure and vacuum. However, to the knowledge of the present authors, no example has been realised where a millimeter-sized 'macroscopic' beam passes from high vacuum to an unenclosed full-atmospheric-pressure environment without intervening windows, mediated solely by differential pumping.

A three-stage differential pumping system was assembled at XOR-CMC at the Advanced Photon Source at Argonne National Laboratory to study the vacuum feasibility of such an approach. It has not yet been tested with X-rays. The assembly is shown schematically in Fig. 1. Utilizing a sequence of commercially available mechanical, turbo-molecular and ion-getter pumps, the system provides a clear beam aperture of 1.37 mm at its most severe constriction point. Turbulent flow through a 'rough' pipe is utilized in the first pumping stage as a strong conductance-limiting mechanism. A beam pipe only 129 mm long is necessary to reduce atmospheric pressure to about 10 mbar. Transmission for hard X-rays by this air column is calculated to be only slightly smaller than that of a standard 250 µm-thick Be window (see Fig. 2). A succeeding second-stage pipe with an internal diameter (ID) of 1.96 mm and a length of 867 mm, driven by a 210 l s^{-1} turbo-molecular drag pump, makes the transition into the high-vacuum region at about 4×10^{-4} mbar, ensuring a stable operating point on the pumping speed plateau of this pump. A third stage, consisting of a beam pipe of 15.7 mm ID and a length of 3430 mm, in combination with a 220 l s^{-1} ion pump, reduces the pressure further into the close-UHV region.

As far as the steady-state vacuum conditions are concerned, the pump assembly introduced above has been found to be stable over a period of days.

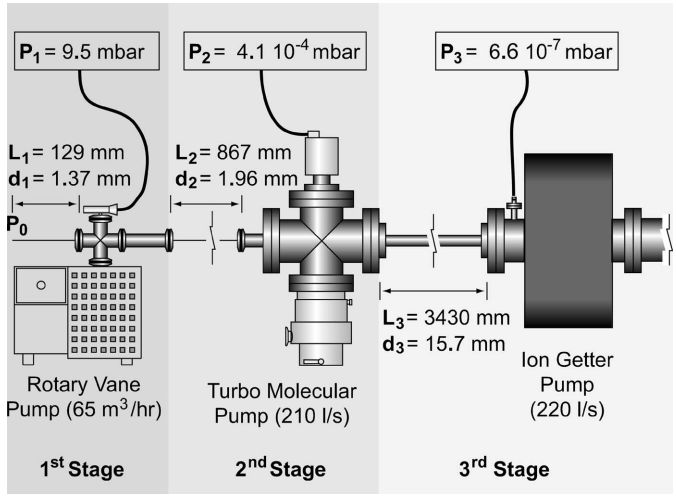

Figure 1
Schematic overview of the three-stage differential pump assembly. Indicated are the length and diameter of the conductance-limiting pipes, type and pumping speed of the associated pumps, and approximate pressures in steady-state operation.

2. Differential pump assembly in detail

2.1. First stage

At the core of the first stage is a single-stage rotary-vane pump of type Leybold 'SOGEVAC', model SV65, with a nominal pumping speed of 65 m^3 h^{-1}. As shown in Fig. 1, a four-way cross, fitted with quick-release couplings of size DN 40, is attached directly to the inlet of the pump to preserve the pumping speed. This cross serves as a vacuum manifold with first and second conductance-limiting X-ray beam pipes mounted on the horizontal ports and a pressure gauge on the top port. As a pressure gauge, a Granville-Phillips 275-type Convectron gauge in connection with a Varian multi-gauge controller is used. It should be noted that the pump used here is an oil-sealed pump which can produce an oil mist. However, large contamination-free dry pumps with similar pumping speeds and pressure ranges are commercially available and should be used in a production device.

The first conductance-limiting beam pipe is made from miniature hypodermic 304 stainless steel tubing. Two types of pipe, referred to as 'smooth' and 'rough', are considered. The smooth pipe consists of an 'as is' length of tubing with an internal diameter d_1 of 1.37 mm and a wall thickness of 0.23 mm. In order to simulate a quantifiable internal surface roughness, a rough pipe is fabricated from 5 mm-long sections of the smooth tubing, inserted at 10 mm intervals into a larger-size tubing with an internal diameter that tightly fits the external diameter of the inserts. The resulting step structure is shown schematically in the insert of Fig. 3. The period of this structure is a compromise between ease of fabrication and having a large number of steps included. In accordance with the height of the steps, an effective roughness amplitude of ε = 0.115 mm is assigned to it. Pipes of both types with various lengths L_1 are mounted on the pump in sequence. The resulting pressure difference between atmospheric pressure P_0 at the open end of the pipe and the pressure P_1 in the manifold is recorded as a function of length and is shown as circles (smooth pipe) and triangles (rough pipe) in Fig. 3. For the final configuration of the pump assembly, a rough pipe with L_1 = 129 mm (circled data point) is chosen, resulting in a pressure of 9.5 mbar. This pressure is close to the lowest value at which the pump maintains its nominal pumping speed of 65 m^3 h^{-1} (see Fig. 4). It should be noted that mechanical pumps, such as the one used here, are inherently stable when pumping on

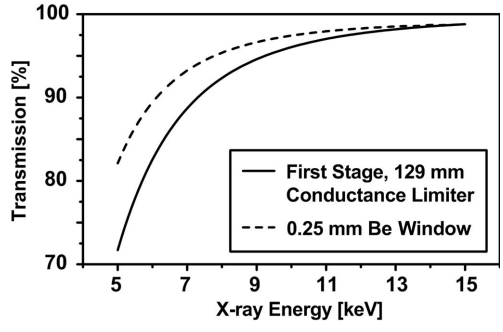

Figure 2
Transmission of hard X-rays as a function of photon energy through the differential pump compared with a standard 250 µm-thick Be window.

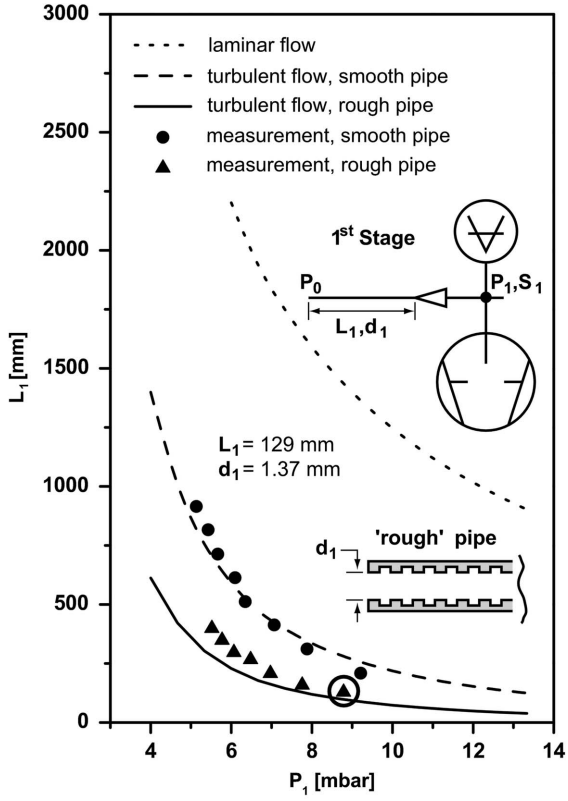

Figure 3
Length of the conductance-limiting pipe as a function of pressure at the low-pressure side of the first stage. The high-pressure side is maintained at atmospheric pressure. Shown are the measurements for a smooth and a rough pipe, together with theoretical predictions based on turbulent flow. For comparison, predictions for laminar flow are also included. The upper insert indicates the circuit diagram of the first stage, including the pipe, pump and pressure gauge. The lower insert shows the structure of the rough pipe. The circled data point corresponds to the chosen operating point of the pump.

open vessels, because an increase in pressure will cause an increase in pumping speed, which in turn counteracts the pressure increase.

A simple theoretical approach, applicable for laminar and turbulent viscous flow, is employed to put these measurements into perspective and help predict the required pipe length L_1 for a specific situation. The viscous flow $q_{\rm pV}$ through the pipe can be approximated (Wutz *et al.*, 1989) by

$$q_{\rm pV}^2 = \frac{1}{f}\frac{\pi^2 d_1^5}{16 L_1}\frac{RT}{M_{\rm molar}}\left(p_0^2 - p_1^2\right). \quad (1)$$

Here, $M_{\rm molar}$, T and R are the molar mass of the gas (air), temperature and ideal gas constant, respectively. The quotient $1/f$ represents the Darcy friction factor, for which explicit approximate expressions have been developed for the various cases of viscous flow:

Laminar flow (Hagen–Poiseuille equation) (Wutz *et al.*, 1989):

$$\frac{1}{f} = \frac{\rm Re}{64}. \quad (2)$$

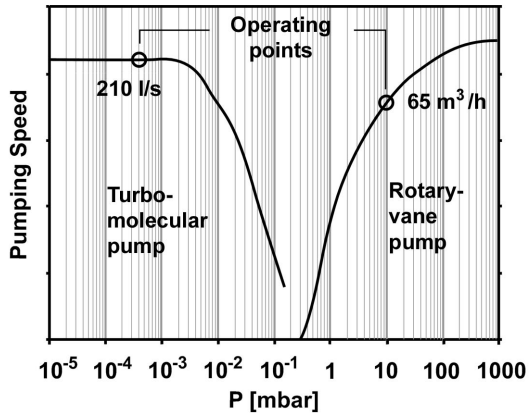

Figure 4
Pumping speed characteristics for the rotary-vane pump and the turbo-molecular pump as supplied by the respective manufacturers. Indicated are the operating points for the pumps in steady-state operation.

Turbulent flow, smooth pipe (Blasius relation) (Livesey, 1998):

$$\frac{1}{f} = \frac{{\rm Re}^{1/4}}{0.316}. \quad (3)$$

Turbulent flow, rough pipe (Haaland, 1983):

$$\frac{1}{f^{1/2}} = -1.8\log_{10}\left[\frac{6.9}{\rm Re} + \left(\frac{\varepsilon}{3.7d}\right)^{1.11}\right]. \quad (4)$$

In these friction factors, Re is the Reynolds number, which is a measure of the degree of turbulence in viscous flow. In terms of the quantities already introduced, it can be written as (Wutz *et al.*, 1989)

$${\rm Re} = \frac{4M_{\rm molar}}{\pi\eta RT}\frac{q_{\rm pV}}{d}. \quad (5)$$

For Re < 2300, viscous flow is considered to be laminar, while for Re > 4000 it is considered to be turbulent, with a transition region between. In the measurements presented in Fig. 3, Re ranges from 6500 at lower pressures to 15000 at higher pressures, making the flow strictly turbulent. In expression (4), the surface roughness ε of the pipe is taken into account explicitly. The authors realise that a large body of more sophisticated work regarding turbulent flow, especially in rough pipes and at large Reynolds numbers, has been assembled (Zagarola & Smits, 1998); however, for the rather basic measurements conducted here, the approximate relations are quite sufficient.

The length L_1 required to achieve a desired pressure p_1 according to (1) with appropriate friction factors is shown graphically in Fig. 3. The measured data for the smooth and rough pipe are adequately reproduced and the effect of lowering the required length by almost a factor of two through employing a rough pipe becomes apparent.

2.2. Second stage

The challenge for the second pumping stage is to bridge the pressure difference between the minimum pressure achieved by the inherently stable first-stage rotary-vane pump and the maximum pressure sustainable by a turbo-molecular drag

pump, which is inherently unstable when operated outside its pumping speed plateau, on a vacuum system with a constant influx of gas. The pumping speed characteristics for the two types of pumps, as supplied by the respective manufacturers, are shown in Fig. 4. For a turbo-molecular pump below its plateau region, a rise in pressure will lead to a decrease in pumping speed, which in turn will lead to a further increase in pressure and eventually to an avalanche towards pumping failure. Thus, care has to be taken to design the second stage in a way that lets the pump operate on its pumping speed plateau, even under pressure fluctuations. For added security, an interlock system should be considered, which monitors the second-stage pressure and valves-off the inlet when a dangerous increase is detected. In the present case, a Pfeiffer TSU 261 turbo-molecular drag pump was employed, capable of generating a constant pumping speed of 210 l s^{-1} down to a pressure of 10^{-3} mbar. Typical gas loads of <0.1 mbar l s^{-1} encountered in the second stage are considered small enough to not cause excessive wear and tear on this kind of pump, as long as adequate cooling is provided.

A theoretical description of the second stage is somewhat difficult, owing to the fact that three different flow regimes are subtended: at the high-pressure side of the conductance-limiting pipe the gas flow is strictly laminar, then proceeds through the transitional regime into the molecular flow regime at the low-pressure side of the stage. Knudsen (1909) was the first to develop an empirical expression for the conductance $C_{\rm trans}$ in transitional flow, which for higher pressures connects smoothly to the laminar region and for lower pressures approaches the molecular regime. It can be written as (Wutz *et al.*, 1989; Knudsen, 1909)

$$C_{\rm trans} = \frac{q_{\rm pV}}{p_1 - p_2} = \frac{\pi d_2^4}{128\eta L_2}\bar{P} + \frac{d_2^3}{3L_2}\left(\frac{\pi RT}{2M_{\rm molar}}\right)^{1/2} \times \frac{1 + (M_{\rm molar}/RT)^{1/2} d\bar{P}/\eta}{1 + 1.235(M_{\rm molar}/RT)^{1/2} d\bar{P}/\eta}. \quad (6)$$

Here, L_2 and d_2 are the length and the diameter of the beam pipe, η is the dynamic viscosity of the gas, while $\bar{P}$ is the average pressure along the pipe. Since the pressure difference generated by the second pumping stage is too large to be adequately represented by a single average pressure value $\bar{P}$, the authors found it more appropriate to numerically integrate the gas flow along the pipe, assuming a linear pressure profile,

$$C = \int_0^{L_2} C_{\rm trans}[p(x)]\,{\rm d}x,$$

with $p(x) = p_1 + (p_2 - p_1)x/L_2$. The result for a series of pipes with internal diameter $d_2 = 1.96$ mm and various lengths L_2 at an inlet pressure of $p_1 = 8.5$ mbar is shown graphically in Fig. 5. The measured data are located between the laminar and molecular flow regimes and are indeed closely approximated by the transitional expression developed as described above. For the final pump configuration a rather long (867 mm) pipe is chosen in favor of accommodating a minimized first-stage conductance limiter and thereby maximizing the overall X-ray transmission. The resulting second-stage steady-state pressure is 4.1 $\times$ 10^{-4} mbar, located solidly on the pumping speed plateau, and allowing long-term stable pump operation.

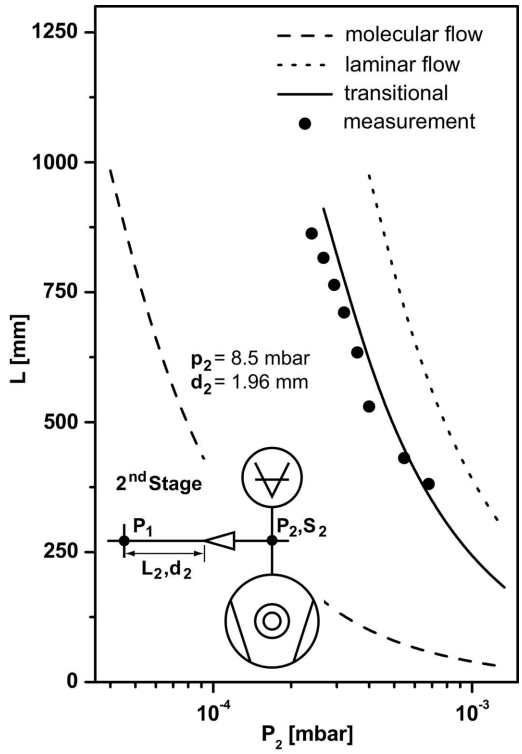

Figure 5
Length of the conductance-limiting pipe as a function of pressure at the low-pressure side of the second stage. Shown are the measurements, together with theoretical predictions based on the integrated transitional flow. For comparison, predictions for laminar and molecular flow are also included. The insert indicates the circuit diagram of the second stage, including the pipe, pump and pressure gauge.

2.3. Third and further stages

Pressures at the core of the third and prospective further stages are in the high- and ultra-high-vacuum region, where gas conductance is governed by a relation for the molecular flow regime (Wutz *et al.*, 1989; Livesey, 1998),

$$L_3 = \frac{d_3^3}{3}\left(\frac{\pi RT}{2M_{\rm molar}}\right)^{1/2} \frac{p_n - p_{n+1}}{S_{n+1}\,p_{n+1}}. \quad (7)$$

Here, $p_n - p_{n+1}$ is the pressure difference across the $(n+1)$th conductance-limiting beam pipe. For the third stage in the present case, a pipe of length $L_3 = 3430$ mm and diameter $d_3 = 15.7$ mm is used, in conjunction with an ion pump of pumping speed $S_3 = 220$ l s^{-1}. The resulting pressure is $p_3 = 6.6 \times 10^{-7}$ mbar, which can be reduced further to any desired final value by additional sequences of pipes and pumps. In fact, differential pumping assemblies are commercially available, designed to bridge the gap between high and ultra-high vacuum (XIA LLC, 2006). Using distributed pumping, local pumping speeds are significantly enhanced here, to allow pressure reductions of five orders of magnitude with a large beam aperture, over a distance of less than a meter.

3. Applications

Besides helping to preserve the coherence of the synchrotron radiation beam, eliminating an exit vacuum window is also expected to be highly beneficial in small-angle X-ray scattering experiments. Parasitic scattering from a material window arises solely from spatial variations of electronic density, *i.e.* defect structures, surface roughness and grain boundaries. This intensity typically increases with decreasing scattering vector q, which corresponds to an increasing size of real space structure. This is shown in Fig. 6 for a 250 µm Be window, a 100 µm CVD diamond window, and a 10 µm mica window (Bösecke & Diat, 1997; Henderson, 1995; Jaski & Cookson, 2007). Thus, a material window often places a lower boundary on the range of scattering vector values accessible. In contrast, the air in the differential pump interface has no structural elements larger than the interatomic distances in the gas, and parasitic scattered intensities remain small even at the lowest accessible values of q. A calculation of the expected parasitic intensities generated by the air column in the first conductance-limiting beam pipe is shown in Fig. 6. It was performed by considering the scattering cross section of an N_2 molecule and integrating it over all molecules present in the air column illuminated by the X-ray beam (Guinier, 1994, ch. 3.1.3).

It is worth noting that parasitic scattering shows no increase below 0.02 Å^{-1}, where the other window materials have an onset of increasing intensity, and absolute intensities of 2.5×10^{-3} sr^{-1} for the differential pump assembly are very small compared with the increasing backgrounds generated by the material windows shown. As a consequence, small-angle X-ray scattering and related techniques with in-air sample environments should greatly benefit from a windowless transition, especially when the samples are weakly scattering in nature.

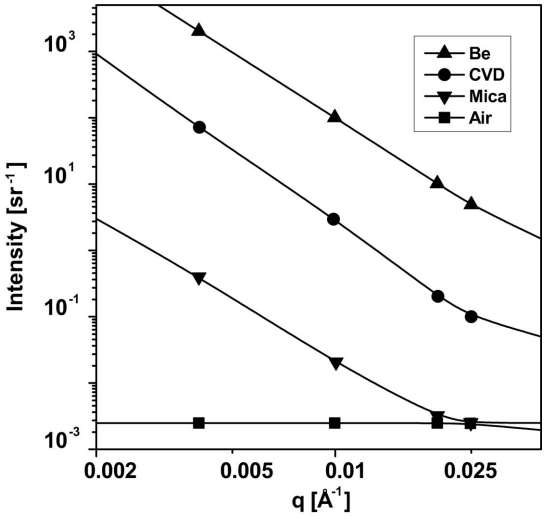

Figure 6
Intensity of parasitic scattering as a function of scattering vector q from various window materials in absolute units. The 'Air' graph is calculated for the present differential pump assembly. For comparison, intensities for a 250 µm Be window, a 100 µm CVD diamond window and a 10 µm mica window as quoted in the literature (Bösecke & Diat, 1997; Jaski & Cookson, 2007) are graphed.

4. Conclusions

A differential pump has been assembled which can provide a windowless transition between an in-air sample environment at atmospheric pressure and a high-vacuum region with an aperture suitable for a synchrotron radiation beamline. Using turbulent flow through a rough pipe as a mechanism for conductance limitation, the distance for the initial pressure reduction can be minimized, and the transmission characteristics for hard X-rays of this short air column are comparable with those of a standard Be window. Simple empirical theoretical expressions are found to be quite adequate in describing the vacuum conditions in all flow regimes and provide a practical means of calculating the parameters of conductance limiters necessary to achieve the desired steady-state pressure distribution throughout the system. The assembly has been tested extensively and was found to be long-term stable when the high-vacuum pumps were allowed to operate on their pumping speed plateaus. A concern is the possible introduction of water vapor into the high-vacuum regions of the pumping system. Unfortunately, no mass spectrometer was available during the measurements to monitor the water contents; however, as a remedy, a cryogenically cooled panel could be included in the pump design, which would effectively trap water vapors. While the mechanical pump used in the present study performed well over periods of days, for extensive long-term operation a pump needs to be chosen that is designed for constant duty at higher pressures in the 10 mbar range.

A fundamental question remains: whether even the air column in the windowless transition might have an adverse effect on the coherence of the X-ray beam or not. In turbulent flow, as present in the first pumping stage, the velocity field of the flowing gas is largely constant in the transverse direction, when averaged over times that are large compared with characteristic periods of turbulent fluctuations. Large changes in velocity only occur in the immediate vicinity of the pipe wall. Thus transverse density and pressure gradients are also very small in the center of the pipe and should have little effect on the X-ray beam.

Nevertheless, while substantial benefits are expected from the use of the differential pump assembly in the context of preserving the X-ray beam coherence and decreasing background parasitic scattering levels, a definite answer to the question above will only be gained through an appropriate experiment conducted with X-rays.

The authors gratefully acknowledge C. Kurtz for making available some of the key equipment used in this study, and C. Kurtz, J. Noonan and A. Khounsari for stimulating discussions about the subject. Work at the Advanced Photon Source is supported by the US DOE, Office of Science, Office of Basic Energy Sciences, under Contract No. DE-AC02-06CH11357.

References

Bösecke, P. & Diat, O. (1997). *J. Appl. Cryst.* **30**, 867–871.
Guinier, A. (1994). *X-ray Diffraction in Crystals, Imperfect Crystals and Amorphous Bodies.* New York: Dover.

Haaland, S. E. (1983). *J. Fluids Eng.* **105**, 89–90.
Henderson, S. J. (1995). *J. Appl. Cryst.* **28**, 820–826.
Hershcovitch, A. (1998). *Rev. Sci. Instrum.* **69**, 868–873.
Hershcovitch, A., Sharma, S., Noonan, J., Rotela, E. & Khounsary, A. (2003). US Patent 6 528 948 B1.
Jaski, Y. & Cookson, D. (2007). *AIP Conf. Proc.* **879**, 1053–1056.
Knudsen, M. (1909). *Ann. Phys.* **28**, 75.
Livesey, R. G. (1998). *Foundations of Vacuum Science and Technology*, edited by J. M. Lafferty, pp. 81–140. New York: Wiley.
Nebiki, T., Hasnat Kabir, M. & Narusawa, T. (2006). *Nucl. Instrum. Methods*, B**249**, 226–229.
Ohashi, H., Ishiguro, E., Tamenori, Y., Kishimoto, H., Tanaka, M., Irie, M., Tanaka, T. & Ishikawa, T. (2001). *Nucl. Instrum. Methods*, A**467–468**, 529–532.
Pinkoski, B. T., Zacharia, I., Hershcovitch, A., Johnson, E. D. & Siddons, D. P. (2001). *Rev. Sci. Instrum.* **72**, 1677–1679.
Snigirev, A., Snigireva, I., Kohn, V. G. & Kuznetsov, S. M. (1996). *Nucl. Instrum. Methods*, A**370**, 634–640.
Sutton, M. (2002). *Third-Generation Hard X-ray Synchrotron Radiation Sources*, edited by D. M. Mills, pp. 101–123. New York: Wiley.
Suzuki, Y., Momose, A. & Sugiyama, H. (1998). *J. Synchrotron Rad.* **5**, 596–599.
Wutz, M., Adam, H. & Walcher, W. (1989). *Theory and Practice of Vacuum Technology*, ch. 4. Braunschweig: Vieweg.
XIA LLC (2006). *Differential Pump Series: DP-0x*, Datasheet at http://www.xia.com/Differential_Pump.html.
Zagarola, M. V. & Smits, A. J. (1998). *J. Fluid Mech.* **373**, 33–79.